Optical coherence tomography of cortical tissue in pilocarpine treated rats as a model for temporal lobe epilepsy

By
Shannon Crowley
Sc.M., Brown University, 2018

Thesis
Submitted in partial fulfillment of the requirements for the degree of Master of Science in the Department of Engineering at Brown University

PROVIDENCE, RHODE ISLAND
MAY 2018

This thesis by Shannon Crowley is accepted in its present form by the Department of Engineering as satisfying the thesis requirements for the degree of Master of Science.

Date:_____ _____
Dr. Jonghwan Lee, Advisor

Date:_____ _____
Dr. Wael Asaad, Reader

Date:_____ _____
Dr. David Borton, Reader

Approved by the Graduate Council

Date:_____ _____
Dr. Andrew G. Campbell, Dean of the Graduate School

Acknowledgements

I would like to thank Dr. Jonghwan Lee for giving me the opportunity to conduct this research in his lab. I am deeply grateful for his knowledge and support. I would also like to thank the entirety of the Lee Lab, however special thanks must go to a select few. To Collin Polucha, for his animal expertise – without whom none of this would have been possible. To Dr. Kyungsik Eom, for his assistance and patience. To Jang-Hoon Lee and Sabina Stefan, for their imaging experience and answering my every question.

I would also like to thank Dr. David Borton and Dr. Wael Asaad for agreeing to be a part of my thesis committee. Thank you for your time, and your contributions to the scientific community at Brown and beyond.

Finally, I would be remiss if I did not thank my family, friends, and Brown community for the undying support I've received over the five years that I've been on campus. It has been an absolute dream.

Table of Contents

List of Figures

List of Tables

Abstract

Epilepsy affects over 3 million people in the United States alone. In many of those cases, the disease is refractory to medication, leaving patients limited in their daily lives. When oral medication does not mitigate or relieve seizure activity, neurosurgery is performed in order to remove the seizure centers of the brain. Herein lies the unmet need in the treatment of this disease. This research is the first step toward creating a novel intraoperative microscope that can delineate the boundary between healthy and epileptogenic tissue in order to assist surgeons in the surgical resection of the diseased tissue in real time. This research aims to use Optical Coherence Tomography (OCT) to quantify the changes before and after seizure activity in cortical tissue. In a rodent model, seizures were induced using pilocarpine and verified by electrocorticography (ECoG). OCT was utilized to quantify the scattering coefficient, blood flow, and the structure of cortical tissue. The optical scattering coefficient of the cortical tissue exhibited a significant increase after the induced seizure activity. This distinct change in the optical property of tissue, which can be detected by OCT in real time and without fluorescence, supports the technical feasibility of the proposed intraoperative microscope.

Introduction

Epilepsy in Humans

In 2015, the CDC estimated that 3 million adults and 470,000 children were living with epilepsy. This equates to 1.2% of the population in the United States [1]. Epilepsy is characterized by recurrent seizures, which involve interrupted brain function caused by increased excitation of neurons [2]. Generalized seizures require emergency treatment, and longer durations of status epilepticus increase the adverse outcomes [3]. The goal of immediate intervention during a seizure is to terminate clinical and electrical signs of status epilepticus, but the underlying cause must be addressed separately [4].

Status epilepticus can present in various cases, such as after a traumatic head injury, in patients with diagnosed epilepsy, or in patients who have never had an unprovoked seizure [4]. Diagnosable epilepsy can be separated into two major categories: symptomatic and idiopathic [5]. Idiopathic epilepsy is genetically transmitted and has no structural markers in the brain, which appears neurologically normal [4,5]. Symptomatic epilepsy is caused by another underlying problem, such as head trauma, neurodegenerative diseases, brain tumor, among others [4,6]. Beyond these two categories, there are 6 different types of seizures, and more than 40 different types of epilepsy that patients can be diagnosed with.

Current treatments and their limitations

Temporal lobe epilepsy (TLE) is the most common type of symptomatic epilepsy in adults, making up 41% of cases [5,6,7]. In patients that suffer from TLE, 2/3 of them present with hippocampal sclerosis, while the remaining 1/3 present with focal limbic lesions [8]. TLE is a type of refractory epilepsy, where patients do not respond to anti-epileptic drugs [9]. Patients with epilepsy suffer from psychological dysfunction, social stigma, and eventually, decreased life

expectancy, outside of the direct effects of a seizure [10]. In cases of refractory TLE, patients undergo surgery to remove the regions of the brain associated with seizure onset [8,10].

Patients who are to undergo neurosurgery first have to undergo a battery of tests. Pre-surgical tests include a neurological examination, magnetic resonance imaging (MRI), ictal video-EEG recordings, and a psychiatric evaluation [10]. Ictal video-EEG recordings allow experts to correlate the onset of seizures both visually and electrically. After surgery, 46-53% of patients were reported to be seizure free [7,11]. This poor outcome might result from the fact that the pre-surgical tests are limited in their ability to accurately identify seizure centers in the brain, making it difficult for surgeons to remove epileptogenic tissue while refraining from damaging healthy brain tissue [12,13,14].

Idea and Objectives

Given the reasons stated above, there is a proven clinical need for an improvement in the characterization technique of epileptogenic tissue. The long-term vision of this project results in the creation of an intraoperative microscope that delivers label-free sub-millimeter resolution differentiation of diseased vs. healthy tissue to better guide neurosurgeons in real time [15]. Toward the long-term goal, this thesis aims to test the idea of imaging status epilepticus with label-free optical methods in a rodent model.

Specifically, these trials will deliver quantifiable changes that occur in the cortex after there has been seizure activity, as observed by OCT imaging techniques. We hypothesize that we will see an increase in blood flow due to heightened seizure activity in the brain. We also hypothesize that there will be an increase in the scattering coefficient of the cortex, associated with changes in the extracellular concentration of ions.

Scientific premise underlying the idea of detection of epileptogenic tissue

The long-term vision of the intra-operative microscope is based on two major physiological paradigms: changes in blood flow and extracellular space constriction. These paradigms have been proven *in vivo* and *in vitro*, and will be able to be visualized using OCT.

Extracellular space constriction has been observed in seizure models both *in vivo* [16-17] and *in vitro* [18,19,20]. Although the mechanism is not yet fully understood, epileptic seizures are known to be accompanied by changes in extracellular concentration of ions [27]. These changes are associated with depolarization of neurons and glial cells, paired with ion flux and water movement from the extracellular space into the intracellular space. During a seizure, there is about a 30% decrease in extracellular space [24]. Extracellular space constriction acts as a positive feedback cycle, leading to an increase intensity of epileptic activity [21,22,23,24].

This extracellular space constriction has been linked to changes in the optical properties of the tissue. Previous work has shown that after global seizure induction, there was an increase in attenuation coefficient of the cortical surface [25]. However, this study was performed in a mice model comparable to petite mal seizures, where we plan to model temporal lobe epilepsy.

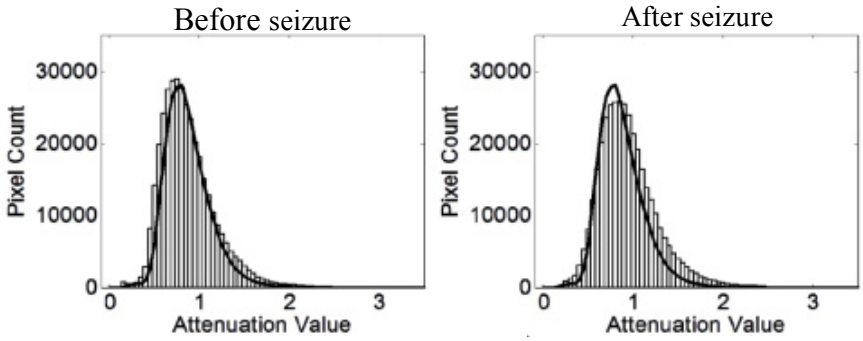

Figure 1: Histogram data of attenuation coefficient before (left) and after (right) global seizure induction using PTZ mouse model. Reprinted from Eberle et al. [25]

Data suggests that in early status epilepticus, there is an increase in cerebral blood flow in regions of the brain with increased activity in order to increase nutrient delivery [26]. Experimental studies have shown that pericytes actively dilate capillaries in the brain [27]. These

studies showed that depolarization leads to contraction of blood vessels, and hyperpolarization leads to dilation. Prior studies report an increase in blood flow for *focal* seizures [28], however changes in blood flow for *global* seizures remain largely unstudied. Such changes in the vasculature and blood flow coupled to neural activation can be visualized as eloquent areas in the exposed cortex during the epilepsy surgery.

Based on these paradigms we expect to distinguish epileptogenic tissue, which should be removed, from normally functioning tissue, which should be preserved, during the epilepsy surgery in real time. This thesis reports the detection of epileptogenic areas with label-free imaging technique, optical coherence tomography, in animal models. Our data will inform future algorithms that are designed to delineate the boundary between healthy and diseased brain tissue in real time.

Technical Background of Optical Coherence Tomography (OCT)

Optical coherence tomography (OCT) was first introduced in the 1990s and is a type of ballistic optical imaging, and their scattering are analyzed [29]. OCT is a non-invasive optical imaging technique that delivers high-resolution label-free images, analogous to ultrasound imaging techniques [30]. OCT uses low coherence interferometry to produce cross-sectional images of the sample that can then be compiled into 3D volumes [31].

The most basic OCT setup based on the Michelson interferometer is shown below in Figure 2 [30]. Beginning at the low coherent light source, the beam goes immediately to the beam splitter. The beam is split 50/50 into sample and reference arms. The sample arm is directed at the sample, where it is reflected back to the beam splitter. Similarly, the reference arm is directed to the reference mirror where it is reflected back to the beam splitter. Both the reflected sample arm and the reflected reference arm are recombined at the beam splitter, and then collected at the detector. When these two beams come back together, the interference pattern results. This pattern

is then reconstructed by the computer to produce the axial profile of the sample (more accurately, the sample's optical field reflectivity).

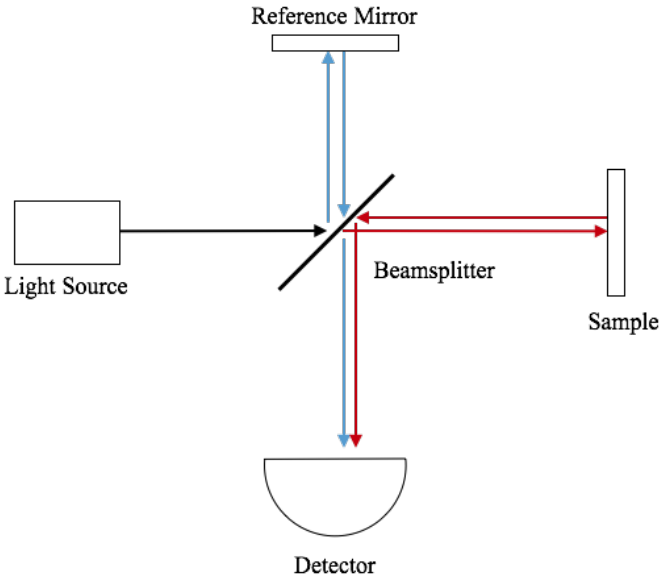

Figure 2: Schematic of a Michelson interferometer in free space. Adapted from Wang et al.[29]

To obtain 3D images of the sample, the sample beam can be scanned in the rater manner. These scans are then reconstructed in the follow manner: first, an A-scan is collected. An A-scan is a 1D array of the voxels in the Z-axis (Fig. 2). A B-scan is a collection of A-scans in the X-axis. The rater scan collects individual B-scans along the Y-axis to reconstruct the complete volumetric scan.

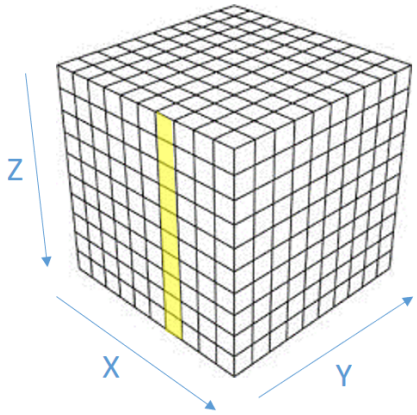

Figure 3: A 3D volumetric scan. First collected is an A-scan, highlighted in yellow. Each small cube represents a voxel, a 3D pixel.

Beyond the described basic structural imaging, recent advances in OCT enable us to image different properties, including vasculature, blood flow, and scattering coefficient.

OCT angiogram delivers high resolution, 3D, label free images of the blood vessels and capillary networks of the brain [32]. Through angiogram images, we hope to visualize changes in blood vessels based on the theory of neurovascular coupling. Doppler OCT combines the basic principles of OCT discussed earlier with the Doppler principle to generate tomographic images of moving components in biological tissue [33]. This technique is used in this study to map blood flow in the brain with single-vessel resolution, to investigate how status epilepticus leads to a change in cerebral blood flow.

Scattering coefficient images are taken to measure the optical properties of the surface of the cortex. Two structural images are taken at two different z depths of the cortex, and then the two 3D images will be analyzed together to produce a 2D map of the tissue scattering coefficient (see the Methods section for details). Because the scattering coefficient of the cortical tissue is known to be related with a range of properties such as the cellular density, cell swelling, and extracellular space, its map will reveal the localized status epilepticus area.

Animal model: Pilocarpine

In rodents, the pilocarpine model is a widely accepted model for human temporal lobe epilepsy [26]. Pilocarpine treatment in rats leads to the eventual development of chronic seizures, marked first by initial status epilepticus, followed by a latent seizure-free time period [34,35]. This model mimics the upregulation of neurotrophins in the hippocampus that is present in humans with TLE, as well as cognitive and memory deficits, while this was beyond the scope of this current study [36]. Pilocarpine also results in lesions in the brain, often appearing in the hippocampus, as temporal lobe epilepsy presents in humans.

It is hypothesized that pilocarpine inhibits the ability of hippocampal cells to buffer the concentration of K+ in the extracellular space. This increased extracellular concentration of K+ has been linked to the initiation of seizure-like activity, as discussed previously [38]. Pilocarpine

is a muscarinic agonist, which, in rats, shows signs of activation such as salivation, piloerection, defecation, and eventually death [8,37]. Because pilocarpine alone has these effects, rats are often pre-treated with a muscarinic antagonist in order to counter these effects. The antagonist will prevent the peripheral effects of pilocarpine, but because it is unable to cross the blood-brain-barrier, the effects of pilocarpine will still be visible in the brain, leading to status epilepticus. This will be discussed further in the Methods section.

The scope of this study will solely focus on the initial status epilepticus. Studies published in literature have shown initial seizure onset to start anywhere from 4 minutes to 45 minutes after pilocarpine injection. For example, Lenz et. al. reported spike activity only 4 minutes after pilocarpine injection (i.p.), followed by a seizure episode that lasted 8-24 minutes [38]. Meanwhile, Turski et al. reported seizure onset to occur between 18-45 minutes after pilocarpine injection (i.p.) [39,40]. Based on these findings, we validate the seizure onset by recording ECoG signals for 40 minutes after pilocarpine injection.

Materials and Methods

Below is a figure outlining the experiment timeline. Throughout the experimentation on many animals (n=23 in total), several iterations were tested in order to find the optimal course of administration. Initially, pilocarpine was being administered via intrahippocampal injection, however intraperitoneal injection proved to be more effective and easier to perform. It was found that there was a higher margin for error with intraperitoneal injection, as there were several instances where the cortex bled after intrahippocampal injection. Additionally, one experiment was performed solely to monitor the vital signs of the rodent throughout the course of the experiment to test the transitions between drugs. More details can be found in Appendix A, outlining all the animal experiments performed.

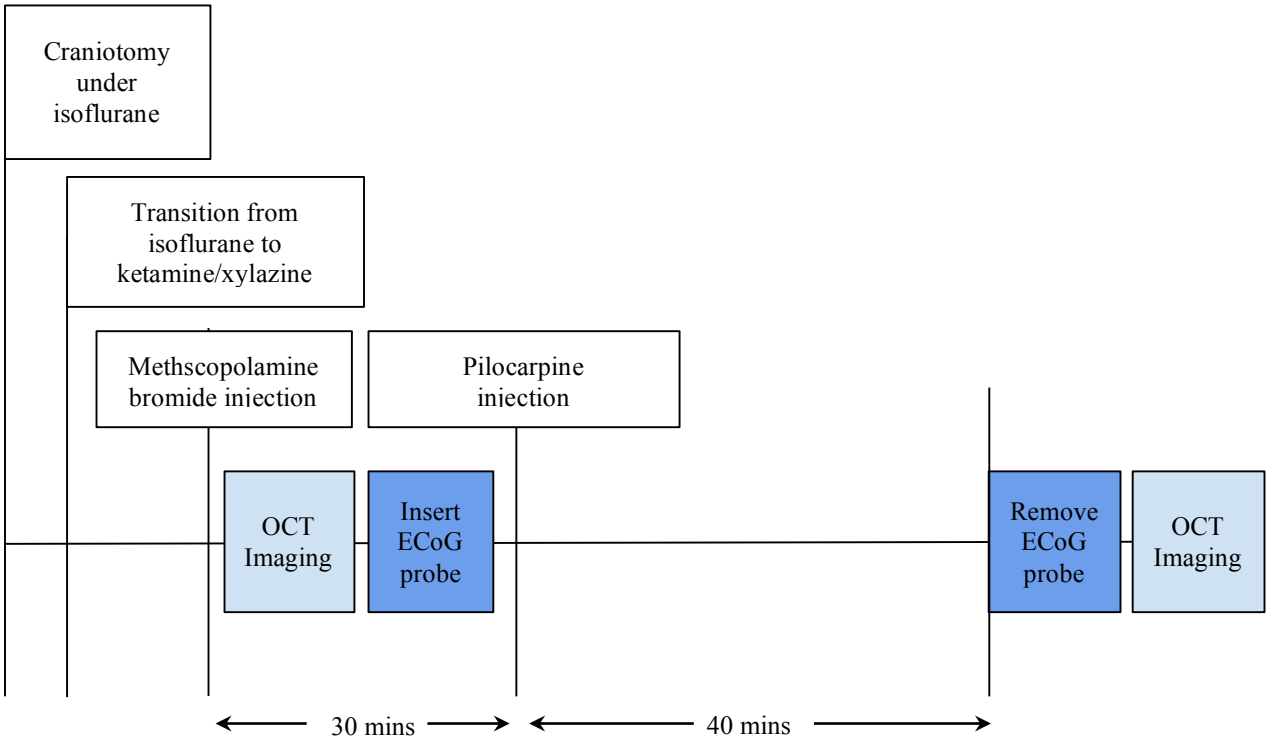

Figure 4: Schematic of experiment timeline. Specific dosages and OCT imaging techniques are further discussed in this section.

Anesthesia

All experiments were approved by the Brown University Institutional Animal Care and Use Committee (IACUC). Adult Sprague-Dawley rats were first anesthetized with isoflurane. Isoflurane is used commonly in rodent models, due to its ease of use and rapid clearance. However, it is a known anti-convulsant [41]. Therefore, only the craniotomy was performed under isoflurane in order to expose the cortex (Figure 5).

The rats were then transitioned to ketamine/xylazine, with boosters administered as needed throughout the experiment. The ketamine/xylazine model is also well established and common for small animals. Ketamine and xylazine have no anti-seizure properties, and status epilepticus has been achieved under this anesthesia [42].

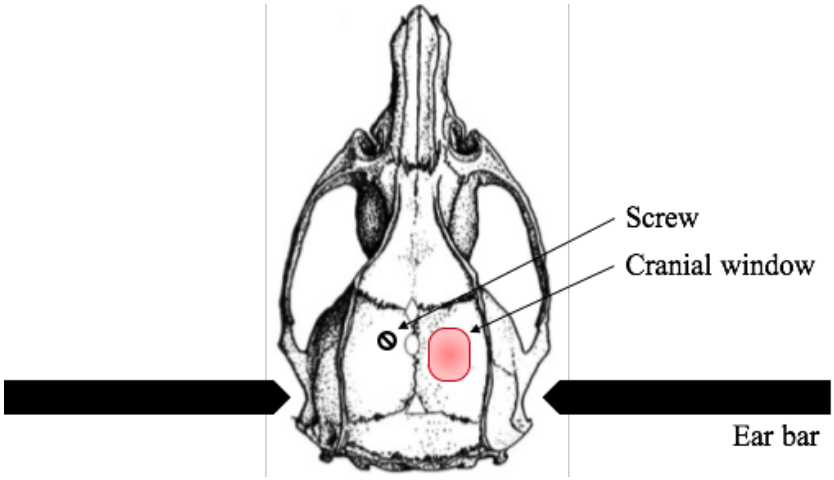

Figure 5: Schematic of craniotomy setup with ECoG screw. The screw serves as the ground electrode, the recording electrode array is placed in the cranial window, as shown in Figure 8.

Pilocarpine and Methscopolamine Bromide

Methscopolamine bromide is first administered (1 mg/kg, i.p.) (Sigma, St. Louis, MO, USA) to prevent the peripheral effects of pilocarpine [43]. 25 minutes later, anesthesia is transitioned between isoflurane and ketamine/xylazeine. Five minutes after the transition between anesthesia drugs, pilocarpine was administered (380 mg/kg, i.p.) (Sigma, St. Louis, MO, USA) [44].

Because methscopolamine bromide drug does not cross blood brain barrier, it will limit the peripheral muscarinic effects of pilocarpine without preventing the achievement of status epilepticus [45,46]. The addition of this drug is necessary because methscopolamine bromide has been shown to prevent the defecation, salivation, and lethality produced by pilocarpine [47,48]. In this model, seizure activity is expected to present within the first 40 minutes after pilocarpine administration.

Data Acquisition

OCT setup and acquisition

After the transition from isoflurane to ketamine/xylazine and the administration of methscopolamine bromide, OCT images were taken before and after status epilepticus, according to the setup in the figure below. The first OCT images will serve as the baseline, to which the second image set taken after seizure activity will be compared. Angiogram, Doppler, and scattering coefficient images were acquired using the LSM03 lens (Thorlabs, Newton, NJ, USA) [49].

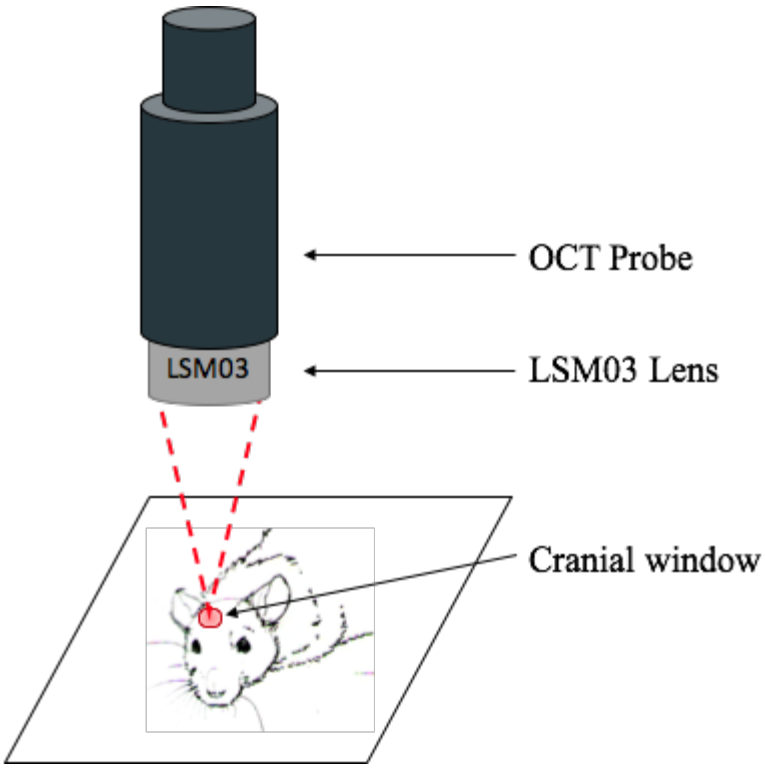

Figure 6: OCT data acquisition schematic.

Images were acquired using the custom Lee Lab application. The app allows for 2D and 3D previews, as well as final image acquisition. Prior to acquisition, certain parameters must be set in the configuration section of the software, as shown in the figure below.

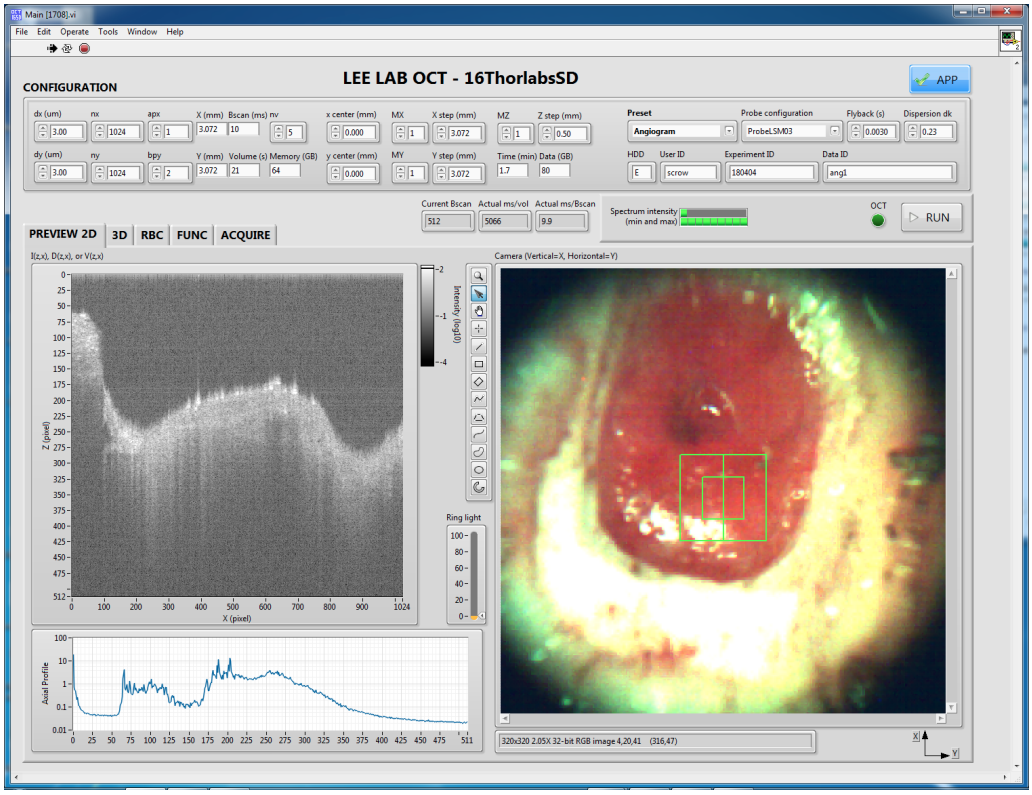

Figure 7: Screenshot of custom Lee Lab software for angiogram OCT (screenshots of other image acquisition settings are shown in Appendix B) dx and dy are the size of the spatial sampling steps in the x and y axis, respectively, in μm. nx and ny are the number of sampling points, again in the x and y directions respectively. apx is the number of repeating A-scans per each x point. For angiogram (ANG) and scattering coefficient (SC) images, apx = 1, but for doppler (DOP), apx = 8. bpy is the number of repeating B-scans per y point, set to 2 for ANG. For DOP and SC, bpy=1. nv is the number of repeating volume scans. For ANG nv = 5, DOP nv = 2, SC nv = 2. X and Y are the total distance that the scan cover in the x or y axis direction (a.k.a., field of view; FOV). For ANG and SC images, X = Y = 3.072 mm. For DOP images, the FOV is X = Y = 1.536 mm. MX, MY, and MZ are the numbers of volume scans in X, Y, and Z, respectively. MX = MY = MZ = 1 for ANG, SC and DOP. The order of volume acquisition is nv > MX > MY > MZ.

Once the parameters have been set, then the image can be previewed using the 3D tab of the application. This preview shows both an image of a single B-scan, along with en face images. The B-scan Y position can be manipulated to visualize different positions within the sample. The projection of the en face images can be set to maximum, average or minimum. Their Z position can also be manipulated along with the depth +/- Z.

Finally, using the Acquire tab of the application, volume data will be collected and written to data files. For angiogram and Doppler OCT images, a single image is captured. However, in order to measure the scattering coefficient two images are captured at two different z

depths, with the second image being vertically translated from the first. These files are then processed using custom Matlab code, which will be explained in the Data Analysis section (pg. 16).

ECoG Data Acquisition

A NeuroNexus "E16-500-5-200-H16" electrode was located on the cortex for ECoG data acquisition as illustrated in Figure 8. The 16-electrode array has a surface area of 1.8x1.97mm^2 and a thickness of 20 μm. An RHD2132 digital electrophysiology interface chip (Intan Technologies, Los Angeles, CA) was used to amplify, filter and record ECoG data. Samples were recorded at a rate of 2 kS/s. Amplifier bandwidth were set to 0.1 Hz and 100 Hz as the lower and upper bandwidth, respectively. A 60-Hz notch filter was also applied to the data.

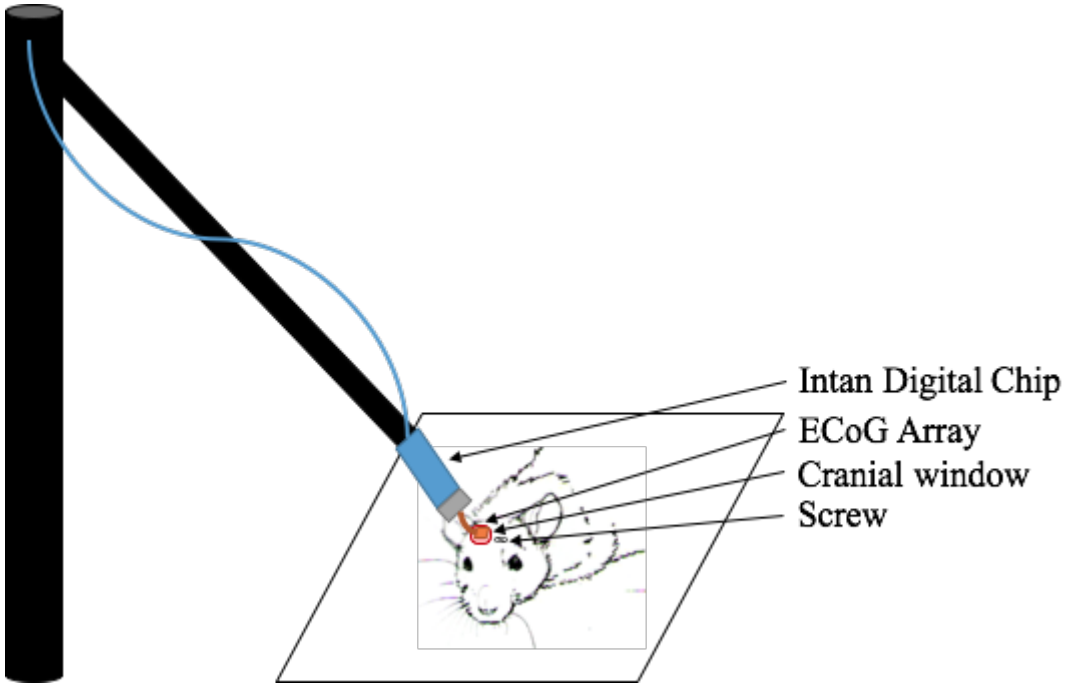

Figure 8: Schematic of ECoG data collection setup.

ECoG data was recorded from minute 0-40 following pilocarpine injection. After this time period, ECoG recording is ceased, and the second OCT image set is acquired. After then, the experiment is halted, and the rodent is euthanized.

Data Analysis

ECoG spectrogram analysis

Raw ECoG data recorded from the RHD2132 series digital electrophysiology interface chip is compared to minimize outlying data. Usually, three different channels were chosen that showed the biggest differences in signals. These channels are compared, both raw data and their spectrograms, and then the single channel with representative data was chosen for further analysis.

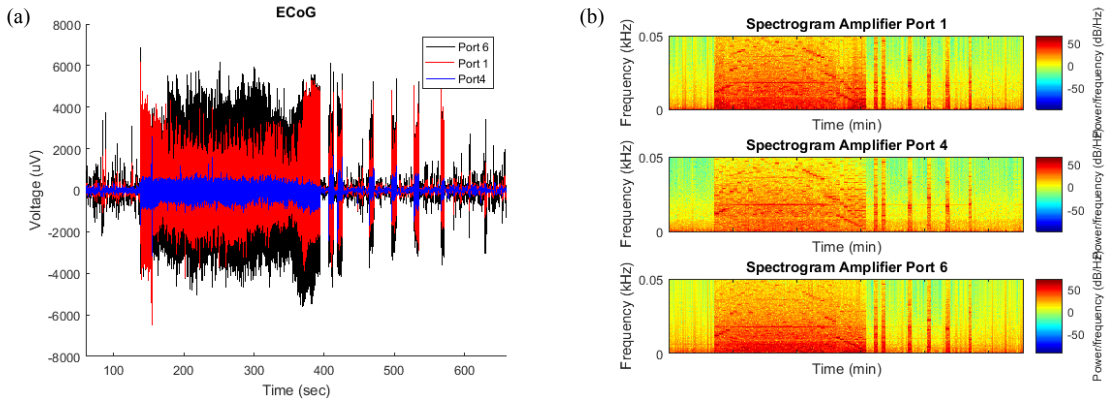

Figure 9: ECoG data selection. (Experiment ID 180328. See Appendix for the serial number of experiments). (a) ECoG raw data plotted from 3 ports. (b) associated spectrograms for each port. For this experiment, port 1 was chosen for analysis.

Raw data is plotted along with the associated spectrograms, similar to methods used by Park et al. [50]. The Matlab function spectrogram returns the short-time Fourier transform of the input signal, in this case the ECoG data. The spectrogram shows the frequency with its associated intensity over time for each minute of the ECoG data. These images will be further discussed in the results section.

OCT data processing

Angiogram data was reconstructed using Lee Lab software which has been coded in Matlab. This software reconstructs and averages angiogram data resulting in both intensity and decorrelation maps. For this experiment, contrast-masked averaging was employed. This technique finds the Y positions that have large motion artifacts and ignores those positions when averaging volumes. In the decorrelation maps, motion artifacts appear as bright horizontal lines with low contrast.

The best way to minimize this motion artifact is to place a glass cover over the cranial window. However, for this experiment in order to gather ECoG data, the cortex needs to be exposed. As a result of this, there is brain movement during OCT imaging due to the animal's cardiac and respiratory motions, resulting in artifacts that cannot be completely removed in post-processing.

After the angiogram has been reconstructed, it can then be visualized and further processed when needed. For example, if there is any tilt in the sample, that can be corrected before the final image is saved. Also, the image can be cropped in the z direction, often to exclude any areas with high reflection. An example of the selection and resulting image can be seen in the figure below.

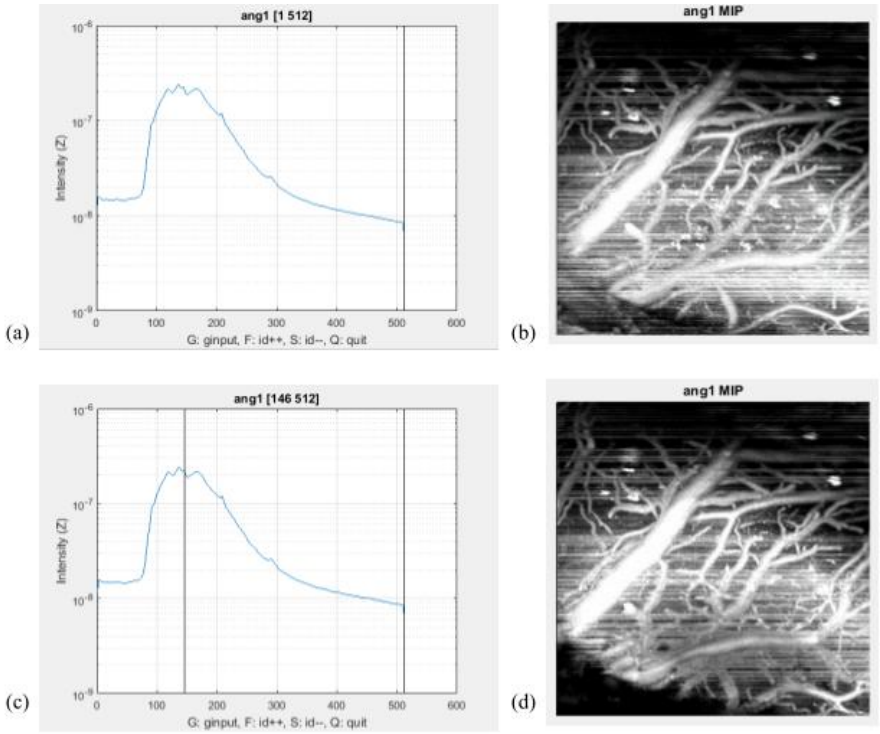

Figure 10: An example of OCT angiogram data processing (experiment ID: 180221). (a) Intensity plot of the associated MIP. By selecting different zz depths, areas with large movement artifacts or high reflection can be eliminated. (b) Reconstructed angiogram MIP from zz [1 512]. (c) Intensity plot with selection of zz [146 512]. (d) Reconstructed angiogram MIP after re-selection of zz.

Image processing to measure the scattering coefficient

The image processing software to measure the scattering coefficient is also done with custom Lee Lab Matlab code. First the images must be cropped, excluding the edges of the image are unusable, shown in the figure below. This crop excludes the part of the image where the surface of the sample drops below a usable z depth.

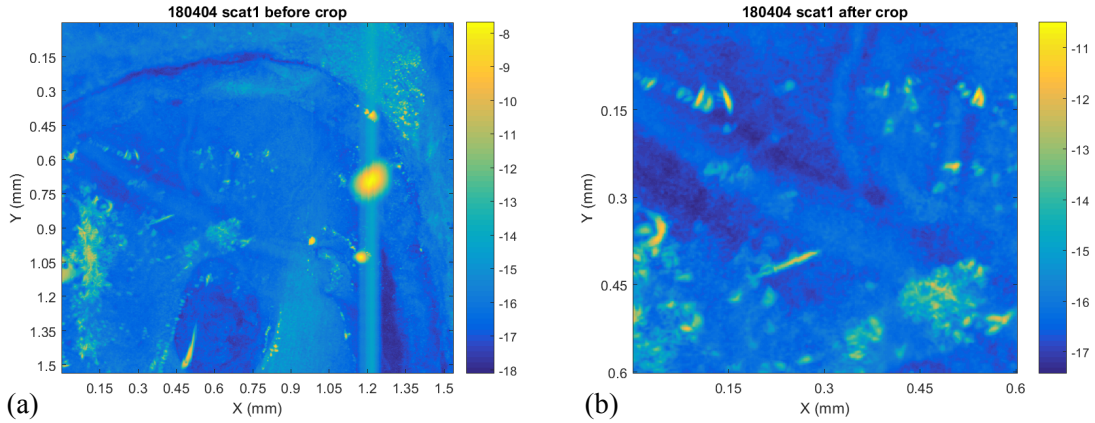

Figure 11: An example of imaging processing for the scattering coefficient measurement (experiment ID: 180404). Scattering coefficient images (a) before cropping and (b) after cropping. This is the cropping for 1 of 2 scattering coefficient OCT images taken before pilocarpine injection. Two more OCT images were taken after seizure activity. The color bar represents the average scattering coefficient for each point in (mm^{-1}). Additional examples of pre- and post-cropping images are shown in the Appendix.

The code takes the two cropped OCT images, one vertically translated about 20-30 pixels from the other, as input. It then shifts each B-scan vertically. Finally, it aligns the vertically translated image with the original image. The resulting image gives a map of the scattering coefficient of the cortex of the rodent's brain. In theory, there will be distinguishable changes between the images taken before and after seizure activity. The mechanisms underlying this change include the alteration in the extracellular space (see Discussion for details). A final reconstructed image is shown in Figure 12. This code also delivers the mean scattering coefficient for the selected region of the cortex.

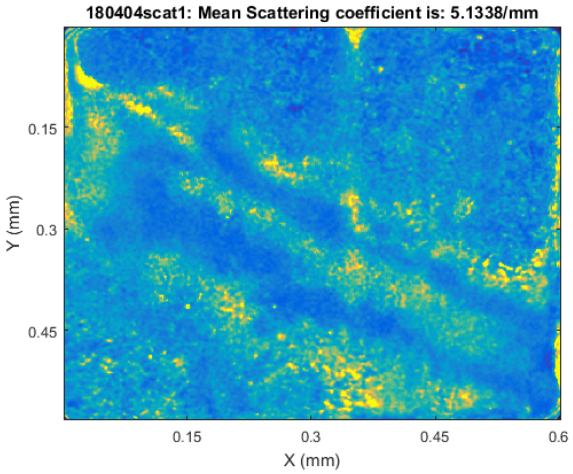

Figure 12: An example of reconstructed scattering coefficient image (experiment ID: 180404), before pilocarpine injection. Mean scattering coefficient is 5.13 mm-1.

Doppler OCT data acquisition and processing

Reconstruction of Doppler images is also done with custom Lee Lab Matlab code. This code analyzes the phase of the consecutive A-scan signals to produce velocity maps. These reconstructed maps are then visualized, shown in the figure below. The velocity maps before and after seizure activity are compared in order to detect changes in blood flow.

In order to calculate absolute blood flow [uL/min] from the velocity map [mm/s], it is best to focus on bright circular dots, rather than longer shapes. The circular shapes correspond to blood vessels that are oriented vertically in the brain. Although we used the area-integral method that is in theory independent of the vessel orientation [51], the vertical orientation leads to more accurate flow readings, due to the nature of A-scans in OCT. Below is a reconstructed Doppler OCT image, which will be further discussed in the results section.

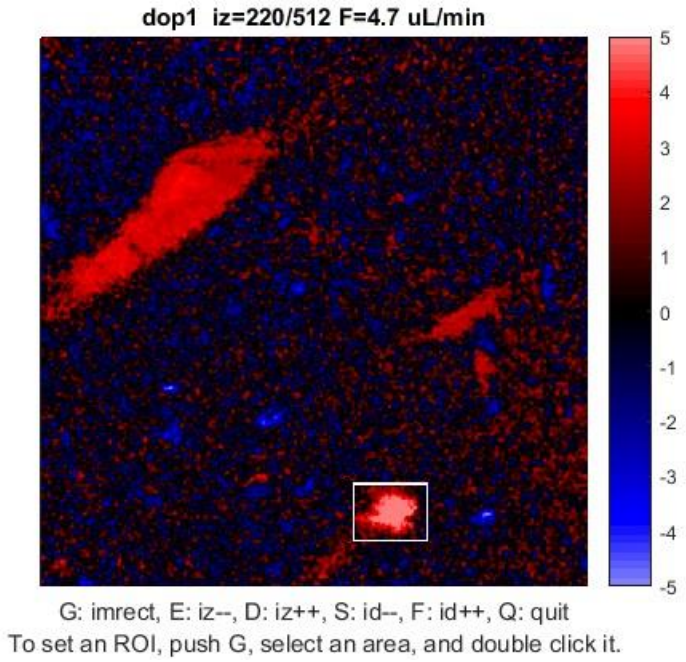

Figure 13: An example of Doppler OCT map of the flow velocity (experiment ID: 180328). This image shows blood flow at a z depth of 220 pixels (equivalent to 770 um from the cortical surface). F gives the volumetric blood flow in uL/min. The color bar represents the range of velocities in mm/s. Arteries are shown in red (flowing into the cortex), and veins are shown in blue (flowing out of the cortex).

Results

This section will primarily focus on the experiments that used the administration of methscopolamine bromide, where the rodent also showed seizure activity. This additional drug completely halted the peripheral effects and high mortality rate that was seen due to pilocarpine.

Table 1: Percent mortality due to pilocarpine. Physical responses in rodents include salivation, changes in breathing, and dropping heart rate. Results divided between experiments that include the administration of methscopolamine bromide, and those that did not.

Percent mortality to pilocarpine Without methscopolamine bromide		Percent mortality to pilocarpine With methscopolamine bromide	
Dead before OCT imaging	11	Dead before OCT imaging	0
Survived until OCT imaging	6	Survived until OCT imaging	4
total	17	total	4
% mortality	64.71%	% mortality	0.00%

Before the addition of methscopolamine bromide, the rodents suffered from adverse reactions such as lacrimation, salivation, defecation, and fatality. Overall, there was a 0% success rate in producing a confirmed seizure episode and a 64.71% mortality rate (n=17). Once methscopolamine bromide was added, induction of seizure activity increased to 50% and mortality dropped to 0% (n=4). Additional experiments in the future should show an improvement in the percent seizure induction, and continuing to have a low mortality rate.

ECoG signal and its spectrogram

As stated in the Methods section, chosen channels of recorded ECoG signals were first compared before analysis; these results will focus on one channel for each experiment. Seizure episodes are marked by rapid high voltage spiking followed by post-ictal depression and slowing of spiking. This change can be seen in the figure below, marked by high voltage spikes approximately 140 seconds after pilocarpine administration.

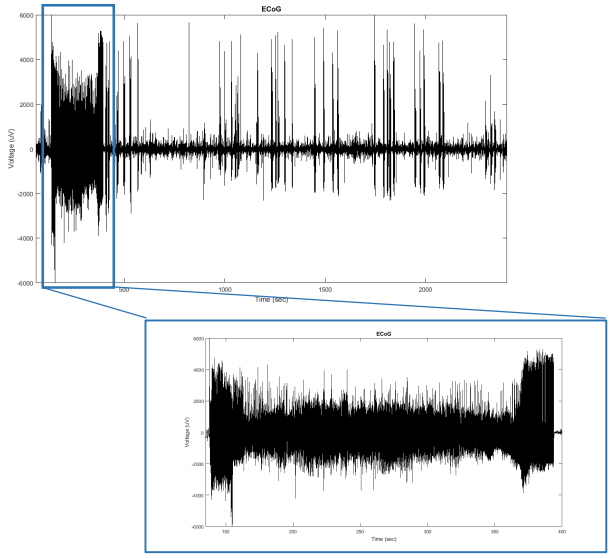

Figure 14: ECoG detection of seizure activity (experiment ID: 180328). (top) The ECoG signal recorded for 40 minutes from the pilocarpine administration. (bottom) Expanded ECoG of seizure episode. Duration 257.3 sec.

This seizure episode can also be verified via spectrogram (Figure 15). Seizure activity presented as a spectrogram has characteristic onset/offset bands. The onset bands can be seen in the expanded spectrogram figure, in the frequency range of 13-17 Hz, for this particular seizure episode. The offset bands can be seen in the frequency range of 3-33 Hz.

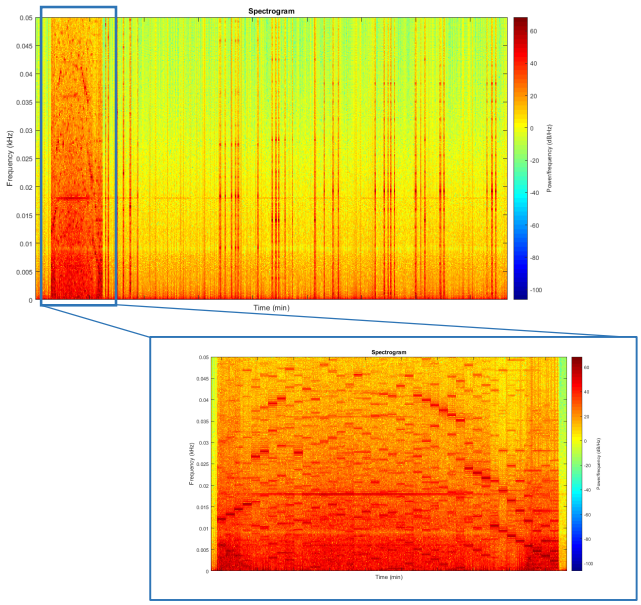

Figure 15: ECoG spectrogram of the seizure activity (experiment ID: 180328). (top) Spectrogram for 40 minutes from the pilocarpine administration. (bottom) Expanded spectrogram of seizure episode. Duration 257.3 sec.

Previous studies have reported that in the pilocarpine seizure model with pretreatment, seizure activity was induced in 75% of animals [8]. For these experiments, pilocarpine-induced seizure activity was visible in 50% of animals that had been pretreated with methscopolamine bromide. In animals that had not been pretreated, no seizures were induced. Additional experiments should improve the percent seizure induction, and this table will be updated as further data becomes available.

Table 2: Percent seizure induction. Seizure episodes have been verified via ECoG analysis as described in the results section. Results divided between experiments that include the administration of methscopolamine bromide, and those that did not. Y = seizure episode visualized, N = no seizure episode.

Percent seizure induction Without methscopolamine bromide		Percent seizure induction With methscopolamine bromide	
n(Y)	0	n(Y)	2
n(N)	17	n(N)	2
total	17	total	4
% seizure	0.00%	% seizure	50%

OCT angiogram image

In order to achieve the best results from angiogram OCT, a glass slip is placed in contact with the brain in order to minimize movement. Because this experiment requires ECoG data collection, we used no glass cover that should be permanently sealed on the craniotomy. For this reason, larger motion artifacts than usual cranial window preparations were observed. These can be reduced in image processing; however, they do not disappear completely. Additional artifacts appear because the surface is not uniformly even and has different areas of reflection.

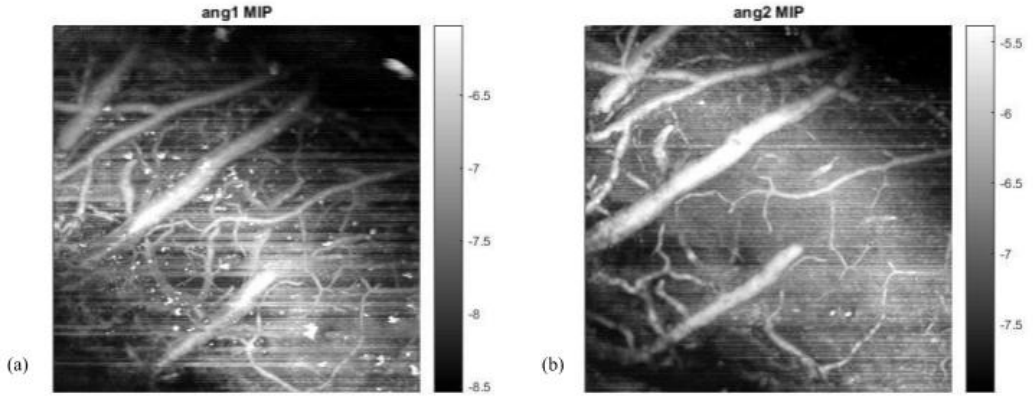

Figure 16: En face maximum intensity projection (MIP) images of OCT angiogram (experiment ID: 180328). (a) Before pilocarpine administration (b) 54 min after pilocarpine administration. Horizontal lines in (a) and (b) are motion artifacts. Bright points in both (a) and (b) are reflection points due to uneven surface.

In the angiogram image after pilocarpine administration, there is a marked decrease in the number of vessels that can be visualized. This supports the hypothesis that after seizure activity there is an increase in the value of the scattering coefficient of the cortical tissue (see the next section). A higher scattering coefficient creates a shadow that hides deeper, narrower vessels, resulting in the difference between the images above.

Scattering coefficient

Analysis of the scattering coefficient maps suggests that the optical scattering coefficient increases after seizure activity. In the first animal, the mean scattering coefficient increased from 2.46 mm^{-1} to 2.99 mm^{-1} (22% increase). In the second animal, the mean scattering coefficient increased from 4.54 mm^{-1} to 5.44 mm^{-1} (20% increase). This data supports the original hypothesis, that constriction of the extracellular space in the cortex occurs by the seizure activity and can lead to an increase in the optical scattering coefficient.

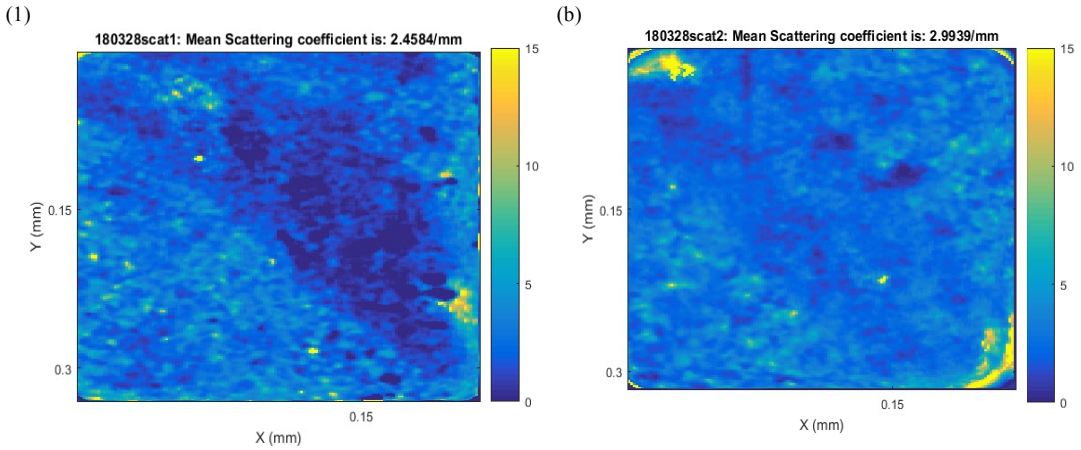

Figure 17: Increased scattering coefficient after the seizure activity (experiment ID: 180328). Reconstructed scattering coefficient images before pilocarpine injection (a) and 40 min later the administration (b). Images before cropping are presented in Appendix B.

The current algorithm that is used to define the surface of the sample is not completely robust. If there are artifacts on the surface of the sample or above the surface, it may define those as being the true surface of the cortex (Figure 18). This leads to problems when converging the two samples and reconstructing this image. In order to combat this issue, small regions of the original images are chosen. However, this does not allow for complete analysis of the entire sample and ultimately leaves out important information.

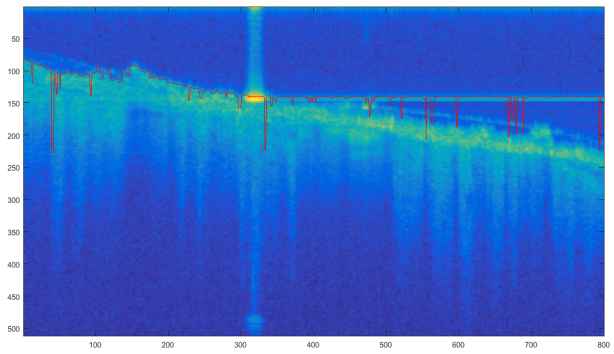

Figure 18: The effect of image artifacts on the automatic identification of the cortical surface (experiment ID: 180328). B-scan at pixel position y=100 (correlates to 350 um from the edge of the field of view). Red line indicates what has automatically been identified as the cortical surface.

In addition to improvement of the surface detection algorithm, specific algorithm development to compare scattering coefficient images will be the next step in working toward the long term goal of an intraoperative microscope. More data will reveal how changes in scattering coefficient values of the surface of the cortex correlate to seizure activity and ultimately show the differences between healthy and diseased tissue. In the long term, this algorithm will need to be able to work in real time.

Cerebral blood flow

Cerebral blood flow has been measured using Doppler OCT images. By selecting the region of interest (ROI), Matlab code calculates the blood flow in that region. Once the ROI is selected, different z depths are explored in order to find peak blood flow in that blood vessel.

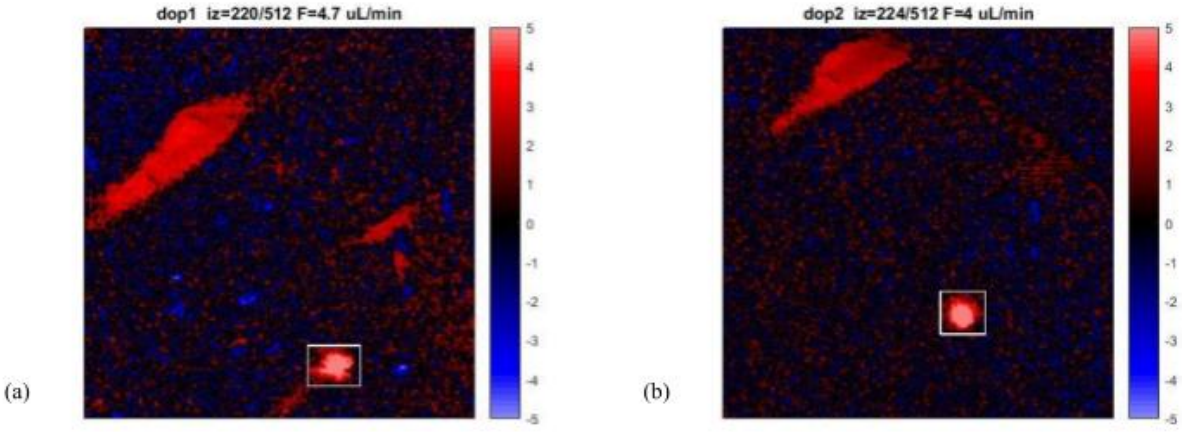

Figure 19: Changes in the arterial blood flow after seizure activity (experiment ID: 180328). (a) Doppler OCT image before pilocarpine injection. ROI at a depth of 770 um. Cerebral blood flow 4.7 uL/min. (b) Doppler OCT image 51 min after pilocarpine administration. ROI at pixel depth of 224. Cerebral blood flow 4 uL/min.

In each region of interest, several (2-3) arteries or veins were selected in each volume, from each rat. These values were then averaged, for arteries and veins respectively, to find the mean blood flow for arteries and veins, before and after seizure activity. From these averages, the percent change in blood flow was calculated, shown in Figure 20.

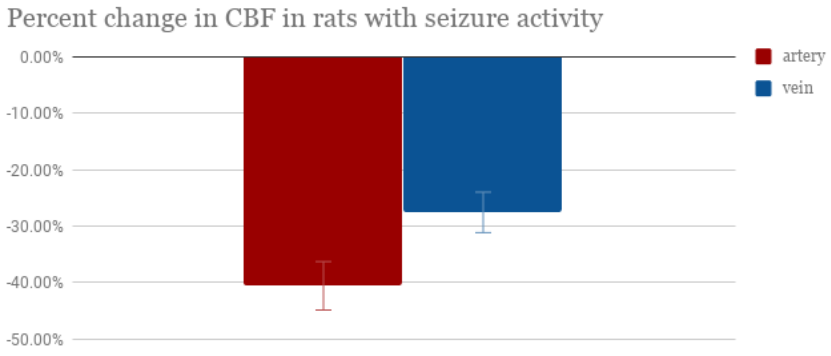

Figure 20: Overall percent change in cerebral blood flow in rodents where seizure activity has been induced. Arteries showed a -40.59±10.62% change in blood flow. Veins showed a -27.55±13.01% change after seizure activity.

It is expected that blood flow increases in the area of *local* seizure activity. However, we induced a *global* seizure in the brain by IP injection, and thus it is not reasonable to expect local blood flow increase in our data. In fact, a few cerebral arterioles selected for flow measurement exhibited a decrease in the flow after seizure activity. This result needs further investigation.

Discussion

The pilocarpine model with methscopolamine bromide pretreatment has induced a seizure in 50 % of rodents. The induced seizures exhibited large variations in the onset time and duration. For example, in one animal, the seizure was induced approximately 2.5 minutes after pilocarpine administration, and lasted 4.5 minutes. Meanwhile, in the other animal, there were two seizure events that were measured via ECoG. The first lasted approximately 3 minutes, with an onset 36 minutes after pilocarpine administration. The second event lasted 3.5 minutes, with an onset 40 minutes after administration. While both of these seizure onset times are within the expected window, they are drastically different. Moving forward, we expect to see an even distribution of seizure onset times within the 40-minute window.

Future work also includes control experiments to study the effect of ketamine on ECoG signals. Ketamine has been known to induce burst firing when administered [52]. Ketamine is a known NMDA receptor antagonist [53]. However, previous literature has shown that pretreatment with MK-801 (a NMDA receptor antagonist) does not block seizure induction in the pilocarpine rodent model [54]. Based on this prior work, ketamine should not interfere with the induction of seizure events, however, further control experiments will show the direct effects.

Future analysis of structural OCT images will include improvement of the head post in order to fix the skull as best as possible to minimize motion artifacts. Additional analysis directly comparing angiograms before and after seizure activity will be done, including changes in vessel diameter.

The paradigm of neurovascular coupling explains how blood flow changes in response to neural activation. In order to measure this, it requires controlled activation, such as whisker stimulation, while measurements are being taken. This method has been employed to characterize baseline blood flow in the brain. These tests will be added in the future, once seizure activity has been characterized robustly and with high reproducibility. This will further characterize the

changes in blood flow that are seen in combination with whisker stimulation and pilocarpine-induced seizure activity.

Currently, the ECoG array that is used in this experiment does not allow for concurrent OCT imaging. Park et al. have developed a graphene-based, carbon-layered electrode array (CLEAR) that can be used for these types of neural applications (Figure 21). Currently, images are being taken prior to pilocarpine injection, and again 40 minutes later. However, with this device, it opens up the possibility of imaging during seizure activity. Currently, in order to alternate between ECoG and OCT setup, the entire OCT probe needs to be moved which can change the z position of the probe as well as the position of the probe within the cranial window.

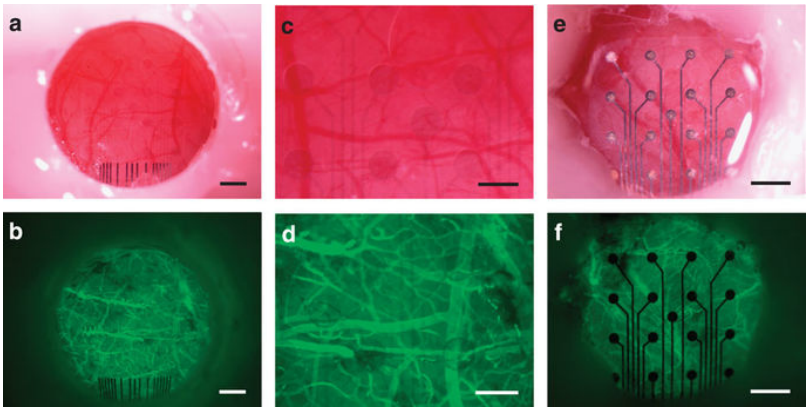

Figure 21: (a) Bright-field image of CLEAR device implanted on the cerebral cortex of a mouse beneath a cranial window. (b) Fluorescence image of same device shown in a. Mouse was given an intravenous injection of fluorescein isothiocyanate–dextran to fluorescently label the vasculature. (c,d) Higher magnification bright-field and fluorescence images of same device shown in a and b, respectively. (e,f) Bright-field and fluorescence images of standard rat-sized micro-ECoG arrays with platinum electrode sites, respectively. Scale bars, 500 µm (a,b), 250 µm (c,d), 750 µm (e,f). In vivo vasculature imaging was repeated in three rats, each with a CLEAR and platinum microECoG array. Images were representative of presented and previously published data Reprinted from Park et al.

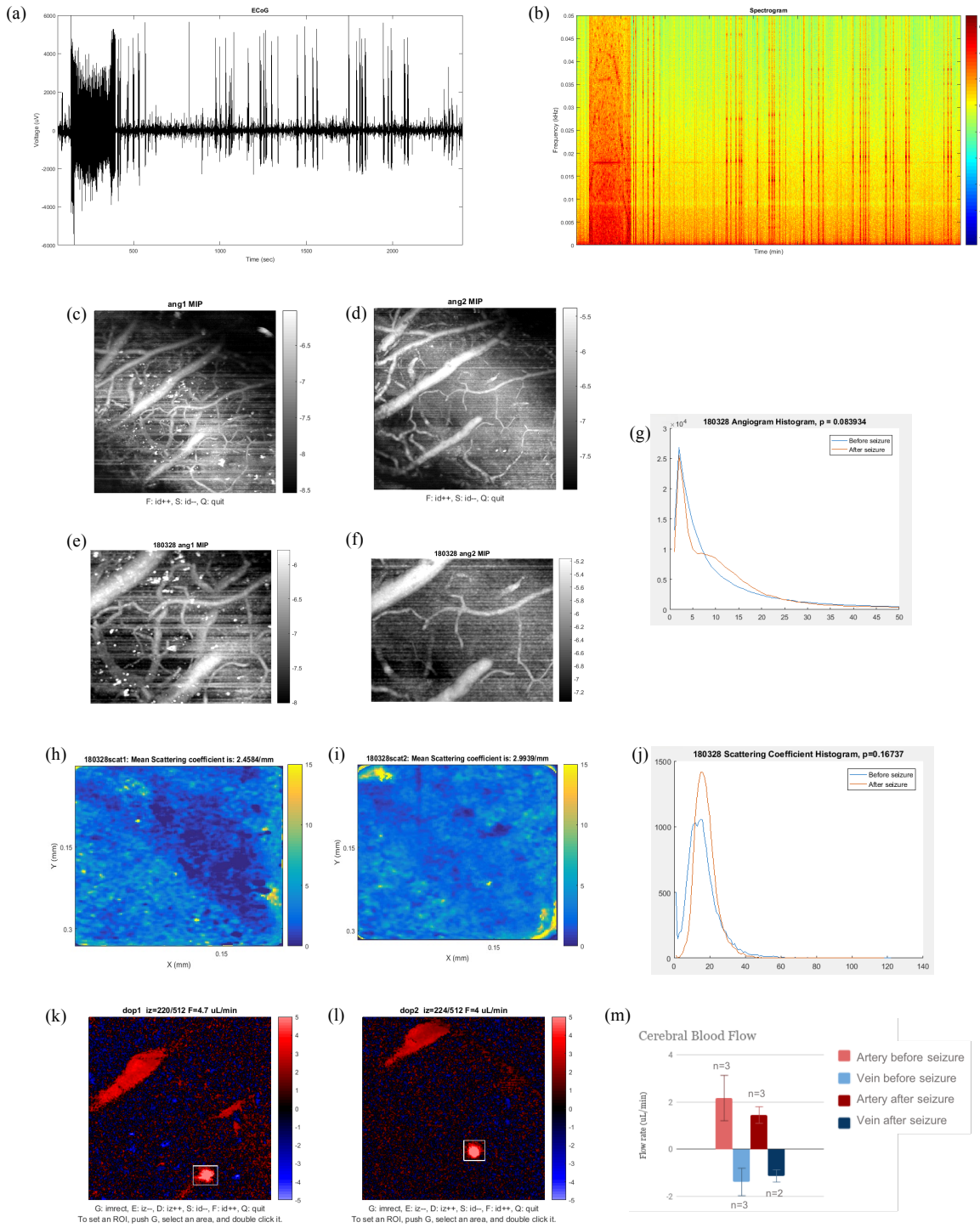

Figure 22: Summary of the result from the first rat (experiment ID 180328). (a) Raw ECoG data for 40 minutes following pilocarpine injection. Seizure activity seen 2 minutes after pilocarpine administration. (b) Spectrogram showing seizure activity. (c) Angiogram before pilocarpine administration. (d) Angiogram after seizure. (e,f) Cropped selections of original angiograms (b,d) respectively. (g) Histogram of (e,f) as ang1 and ang2 in the legend indicate those before and after seizure, respectively. (h,i) Scattering coefficient maps before (scat1) and after (scat2) seizure activity. (j) Histogram of scat1 and scat2. (k,l) Doppler images before and after seizure, with boxes showing ROI where the absolute blood flow (uL/min) was calculated. (m) Cerebral blood flow before (dop1) and after (dop2) seizure for both arteries and veins.

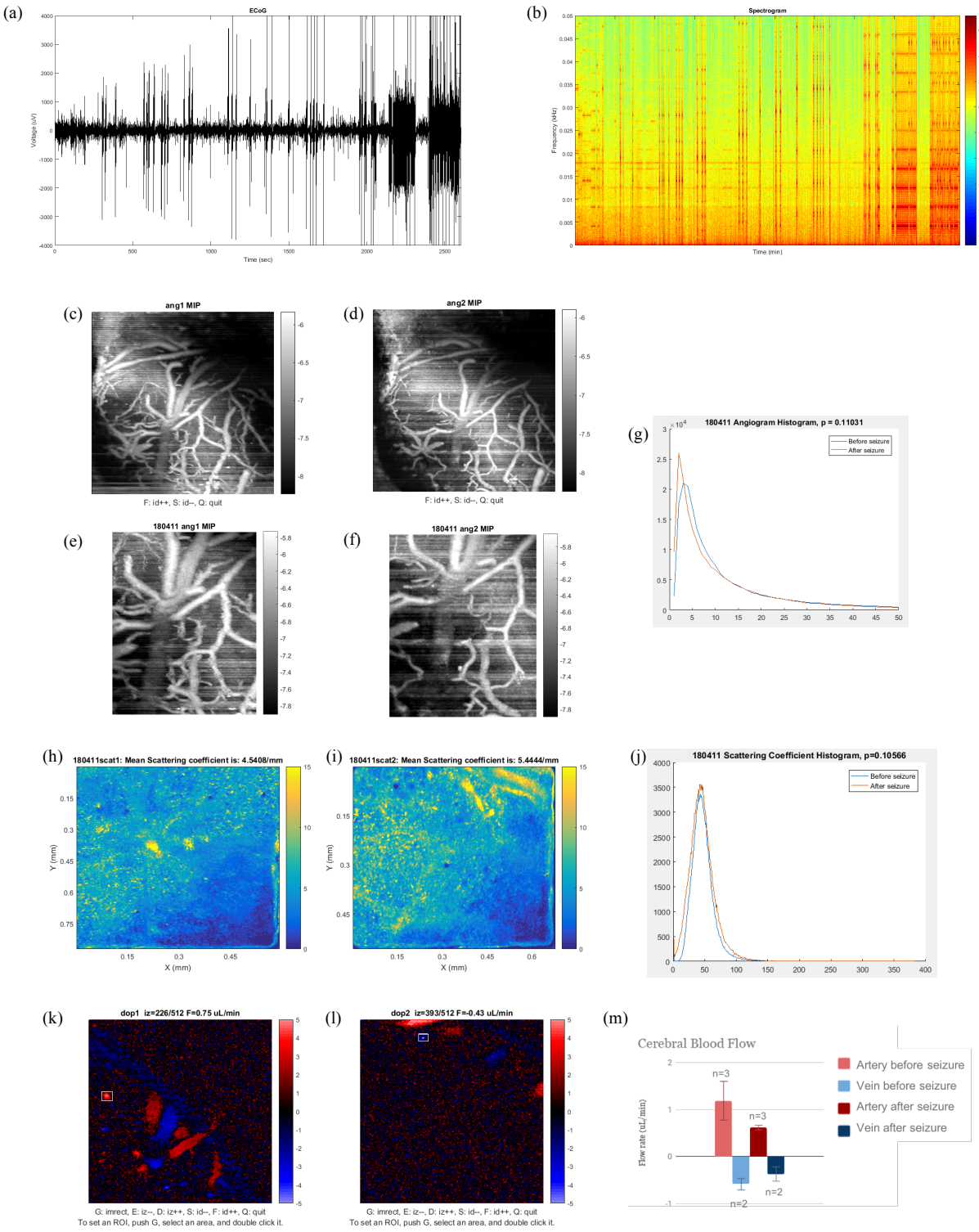

Figure 23: Summary of the result from the second rat (experiment ID 180411). (a) Raw ECoG data for 40 minutes following pilocarpine injection. Seizure activity seen 2 minutes after pilocarpine administration. (b) Spectrogram showing seizure activity. (c) Angiogram before pilocarpine administration. (d) Angiogram after seizure. (e,f) Cropped selections of original angiograms (b,d) respectively. (g) Histogram of (e,f) as ang1 and ang2 in the legend indicate those before and after seizure, respectively. (h,i) Scattering coefficient maps before (scat1) and after (scat2) seizure activity. (j) Histogram of scat1 and scat2. (k,l) Doppler images before and after seizure, with boxes showing ROI where the absolute blood flow (uL/min) was calculated. (m) Cerebral blood flow before (dop1) and after (dop2) seizure for both arteries and veins

Conclusion

This study has successfully induced seizure activity in the rat pilocarpine model as verified by the ECoG recording. OCT imaging has allowed for quantification of the changes in optical properties associated with this seizure activity. The optical scattering coefficient of the cortical tissue exhibits a significant increase after the seizure. This increase also leads to a decrease in visibility of blood vessels in the OCT angiogram images. Doppler OCT enables us to quantify cerebral blood flow at single vessel resolution in vivo, and its data suggests that overall cerebral blood flow decreases (in both arteries and veins) by the global seizure.

The biggest challenge during these trials has been to reliable produce seizure activity in the rodents. The addition of methscopolamine bromide has visibly improved the peripheral effects of pilocarpine that were present during previous trials, with salivation and defecation being the two most obvious. As more trials are being run with methscopolamine bromide, the incidence of seizure onset should improve. Additionally, the differences in the brain before and after seizure activity are expected to become more evident.

In the future, changes in blood flow as imaged by Doppler OCT will reveal a pattern that will inform how the brain functions as a result of seizure activity. After a more robust software can be developed, the same can be said for the analysis of scattering coefficient and angiogram images.

Once these patterns are identified, the associated software will be able to be developed to identify these differences in real time. Ultimately, these trials are the beginnings of research that will be able to inform clinical decisions that are made in the operating room and improve the outcome of the epilepsy surgery.

References:

[1] Zack, M.M. and R. Kobau, *National and State Estimates of the Numbers of Adults and Children with Active Epilepsy — United States, 2015.* MMWR Morb Mortal Wkly Rep 2017. **66**(31): p. 821-825.

[2] Raimondo, J.V., et al., *Ion dynamics during seizures.* Front Cell Neurosci, 2015. **9**: p. 419.

[3] Lowenstein, D.H., T. Bleck, and R.L. Macdonald, *It's Time to Revise the Definition of Status Epilepticus.* Epilepsia, 1990. **40**(1): p. 120-122.

[4] Epilepticus, W.G.o.S., *Treatment of Convulsive Status Epilepticus: Recommendations of the Epilepsy Foundation of America's Working Group on Status Epilepticus.* 1993. **270(**7): p. 854-59.

[5] Engel Jr., J., *Introduction to temporal lobe epilepsy.* Epilepsy Research, 1996(26): p. 141-150.

[6] Kobayashi, M.W., X.; Buckmaster, P. S., *Reduced Inhibition and Increased Output of Layer II Neurons in the Medial Entorhinal Cortex in a Model of Temporal Lobe Epilepsy.* The Journal of Neuroscience, 2003. **23**(24): p. 8471-8479.

[7] Curia, G., et al., *Pathophysiogenesis of Mesial Temporal Lobe Epilepsy: Is Prevention of Damage Antiepileptogenic?* Current Medicinal Chemistry, 2014(21): p. 663-688.

[8] Mora, Graciela Navarro, et al. "Does pilocarpine-induced epilepsy in adult rats require status epilepticus?." PloS one 4.6 (2009): e5759.

[9] Laxer, K.D., et al., *The consequences of refractory epilepsy and its treatment.* Epilepsy Behav, 2014. **37**: p. 59-70.

[10] Jutila, L., et al., *Long term outcome of temporal lobe epilepsy surgery: analyses of 140 consecutive patients.* 2002(73): p. 486-494.

[11] Falconer, M.A. and E.A. Serafetinides, *A follow-up study of surgery in temporal lobe epilepsy.* J. Neruol. Neurosurg. Psychiat., 1963(26): p. 154-165.

[12] Duncan, J., *Imaging in Epilepsy.* Brain, 2997(120): p. 339-77.

[13] Bookheimer, S., *Functional MRI applications in clinical epilepsy.* Neuroimage, 1996(4): p. S139-S146.

[14] Spencer, S., *The relative contributions of MRI, SPECT, and PET imaging in epilepsy.* Epilepsia, 1994(6): p. S72-S89.

[15] Lee, J., *Clinical Intraoperative Dynamic Microscope: Proof of Concept.*

[16] Traynelis, S. and R. Dingledine, *Role of extracellular space in hyperosmotic suppression of potassium induced electrographic seizures.* J Neurophysiol, 2989(61): p. 927-38.

[17] Roper, S., A. Obenaus, and F. Dudek, *Osmolality and nonsynaptic epileptiform in rat CA1 and dentate gyrus.* Ann Neurol, 1992(31): p. 81-5.

[18] Binder, D., et al., *In vivo measurement of brain extracellular space diffusion by cortical surface photobleaching.* J Neurosci, 2004(24): p. 8049-56.

[19] Lux, H., U. Heinemann, and I. Dietzel, *Ionic changes and alterations in the size of the extracellular space during epileptic activity.* Adv Neurol, 1986(44): p. 619-39.

[20] Heinemann, U. and I. Dietzel, *Extracellular potassium concentration in chronic alumina cream foci of cats.* J Neurophysiol, 1984(52): p. 421-34.

[21] Binder, Devin K., et al. "Increased seizure duration and slowed potassium kinetics in mice lacking aquaporin-4 water channels." Glia 53.6 (2006): 631-636.

[22] Dudek, F. Edward, Andre Obenaus, and Jeffrey G. Tasker. "Osmolality-induced changes in extracellular volume alter epileptiform bursts independent of chemical synapses in the rat: importance of non-synaptic mechanisms in hippocampal epileptogenesis." Neuroscience letters 120.2 (1990): 267-270.

[23] Roper, Steven N., Andre Obenaus, and F. Edward Dudek. "Osmolality and nonsynaptic epileptiform bursts in rat CA1 and dentate gyrus." Annals of neurology 31.1 (1992): 81-85.

[24] Chebabo, S. R., et al. "Interstitial space, electrical resistance and ion concentrations during hypotonia of rat hippocampal slices." The Journal of physiology 487.3 (1995): 685-697.

[25] Eberle, Melissa M., et al. "Localization of cortical tissue optical changes during seizure activity in vivo with optical coherence tomography." *Biomedical optics express* 6.5 (2015): 1812-1827.

[26] Choy, M., et al., *Cerebral blood flow changes during pilocarpine-induced status epilepticus activity in the rat hippocampus.* Experimental Neurology, 2010. **225**(1): p. 196-201.

[27] Attwell, D., et al., *Glial and neuronal control of brain blood flow.* Nature, 2010. **468**(7321): p. 232-243.

[28] Theodore, W. H., et al. "Effect of Seizures on Cerebral Blood Flow Measured with 15–H2O and Positron Emission Tomography." *Epilepsia* 37.8 (1996): 796-802.

[29] Wang, Lihong V., and Hsin-I. Wu. Biomedical optics: principles and imaging. John Wiley & Sons, 2012.

[30] Podoleanu, A. Gh. "Optical coherence tomography." Journal of Microscopy 247.3 (2012): 209-219.

[31] Huang, David, et al. "Optical coherence tomography." science 254.5035 (1991): 1178-1181.

[32] Musat, Ovidiu, et al. "New perspectives in retinal imaging-angio OCT." Romanian journal of ophthalmology 60.2 (2016): 63.

[33] Liu, Gangjun, and Zhongping Chen. "Advances in Doppler OCT." Chinese Optics Letters 11.1 (2013): 011702.

[34] Curia, G., et al., *The pilocarpine model of temporal lobe epilepsy.* Journal of Neuroscience Methods, 2008. **172**(2): p. 143-157.

[35] Kohling, R., et al., *Extracellular potassium elevations in the hippocampus of rats with long-term pilocarpine seizures.* Neuroscience Letters, 1995(201): p. 87-91.

[36] Kandratavicius, Ludmyla, et al. "Animal models of epilepsy: use and limitations." Neuropsychiatric disease and treatment 10 (2014): 1693.

[37] Witkin, J.M., et al., *Nonmuscarinic Neurotoxicity of Oxotremorine.* The Journal of Pharmacology and Experimental Therapeutics, 1987. **241**(1): p. 34-41.

[38] Lenz, Maximilian, et al. "Pilocarpine-induced status epilepticus is associated with changes in the actin-modulating protein synaptopodin and alterations in long-term potentiation in the mouse hippocampus." Neural plasticity 2017 (2017).

[39] Tetz, Lauren M., et al. "Development of a rat pilocarpine model of seizure/status epilepticus that mimics chemical warfare nerve agent exposure." Toxicology and industrial health 22.6 (2006): 255-266.

[40] Turski, Waldemar A., et al. "Limbic seizures produced by pilocarpine in rats: behavioural, electroencephalographic and neuropathological study." Behavioural brain research 9.3 (1983): 315-335.

[41] Choy, M., et al., *Cerebral blood flow changes during pilocarpine-induced status epilepticus activity in the rat hippocampus.* Experimental Neurology, 2010. **225**(1): p. 196-201.

[42] Englot, D.J., et al., *Remote effects of focal hippocampal seizures on the rat neocortex.* J Neurosci, 2008. **28**(36): p. 9066-81.

[43] Glien, M.B., C.; Potschka, H,; Voigt, H.; Ebert, U.; Loscher, W., *Repeated low-dose treatment of rats with pilocarpine: low mortality but high proportion of rats developing epilepsy.* Epilepsy Research, 2001(46): p. 111-119.

[44] Garcia-Cairasco, N., et al., *Neuroethological study of status epilepticus induced by systemic pilocarpine in Wistar audiogenic rats (WAR strain).* Epilepsy Behav, 2004. **5**(4): p. 455-63.

[45] Witkin, J. M., et al. “Nonmuscarinic neurotoxicity of oxotremorine.”; Journal of Pharmacology and Experimental Therapeutics 241.1 (1987): 34-41.

[46] Feldman, Joseph A., and Bruce J. Robb. “;Colorimetric determination of atropine, homatropine, scopolamine, and their derivatives by the ferric hydroxamate method.”; Journal of pharmaceutical sciences 59.11 (1970): 1646-1647.

[47] Witkin, J. M., et al. “;Nonmuscarinic neurotoxicity of oxotremorine.”; Journal of Pharmacology and Experimental Therapeutics 241.1 (1987): 34-41.

[48] Curia, G., et al., *The pilocarpine model of temporal lobe epilepsy.* Journal of Neuroscience Methods, 2008. **172**(2): p. 143-157.

[49] "Scan Lenses for OCT Imaging - Thorlabs, Inc.." https://www.thorlabs.com/newgrouppage9.cfm?objectgroup_id=10343. Accessed 2 Mar. 2018.

[50] Park, Yun S., et al. "Seizure detection on/off system using rats' ECoG." Engineering in Medicine and Biology Society (EMBC), 2012 Annual International Conference of the IEEE. IEEE, 2012.

[51] Srinivasan, V. J., Sakadzic, S., Gorczynska, I., Ruvinskaya, S., Wu, W., Fujimoto, J. G. & Boas, D. A. Quantitative cerebral blood flow with optical coherence tomography. *Opt. Express* **18,** 2477–2494 (2010).

[52] Hunt, Mark J., et al. "Differential effects produced by ketamine on oscillatory activity recorded in the rat hippocampus, dorsal striatum and nucleus accumbens." *Journal of Psychopharmacology* 25.6 (2011): 808-821.

[53] Cunha, Alexandra Olimpio Siqueira, et al. "Neuroprotective Effects of Diazepam, Carbamazepine, Phenytoin and Ketamine after Pilocarpine-induced Status Epilepticus." *Basic & clinical pharmacology & toxicology* 104.6 (2009): 470-477.

[54] Rice, Ann C., and Robert J. DeLorenzo. "NMDA receptor activation during status epilepticus is required for the development of epilepsy." *Brain research* 782.1-2 (1998): 240-247.

Appendix A

Table A 1: Experiment outcomes. Pilocarpine = pilo, Methscopolamine bromide = meth-br.

Experiment date	Protocol	OCT (Y/N)	ECoG (Y/N)	ECoG recording method	Pilo dose	Meth-br dose	Result	Seizure episode (Y/N)	Seizure episode duration (sec)	Mortality due to pilo
2017/06/13	IH	N	Y	5 min pre 1/5 min post	2.4mg/µL	--	Brain bleed due to micropipette injection	--	--	--
2017/06/20	IP	N	Y	5 min pre 1/5 min post	340 mg/kg	--	Stopped breathing at 31 min	N	--	Y
2017/07/11	IP	N	Y	5 min pre 1/5 min post	340 mg/kg	--	Stopped breathing at 38 min	N	--	Y
2017/09/27	IH	N	Y	5 min pre 1/5 min post	2.4mg/µL	--	Stable vitals 65 min post-pilocarpine injection	N	--	N
2017/09/27	IH	N	N *	5 min pre 1/5 min post	2.4mg/µL	--	Stable vitals 65 min post-pilocarpine injection	N	--	N
2017/10/04	--	--	--	5 min pre 1/5 min post	--	--	--	--	--	--
2017/10/11	IH	N	Y	5 min pre 1/5 min post	2.4mg/µL	--	Stable vitals 55 min post-pilocarpine injection	N	--	N
2017/10/25	IP	N	Y	5 min pre 1/5 min post	340 mg/kg	--	Stable vitals 45 min post-pilocarpine	N	--	N
2017/11/15	60 min no pilo IP	N N	Y Y	5 min pre 1/5 min post 5 min pre 1/5 min post	X 380 mg/kg	-- --	Stable vitals for 60 minutes (min 8) drooling (min 35) convulsions	N N	-- --	Y Y

							(min 41) stopped breathing, resumed (min 44) stopped breathing			
2017/11/29	IP	N	Y	5 min pre 1/5 min post	380 mg/kg	--	(min 26) heart rate dropped, experiment ended	N	--	Y
2017/11/29	IP	N	Y	5 min pre 1/5 min post	380 mg/kg	--	(min 4) stopped breathing, experiment ended	N	--	Y
2017/12/6	IP	N	Y	3 min pre 1/5 min post (until 20) Continuous post	380mg/kg	--	(min 5) drooling (min 29) stopped breathing, resumed on its own (min 36) stopped breathing, experiment ended	N	--	Y
2017/12/13	IP	N	Y	5 min pre 1/5 min post (until 20) Continuous post	380mg/kg	--	(min 3) drooling Stable vitals through (min 60), no change inECoG	N	--	N
2017/12/20	IP	N	Y	5 min pre 1/5 min post (until 20) Continuous post	380mg/kg	--	(min 2) drooling (min 17) heavy breathing (min 55) stopped breathing, experiment ended	N	--	Y
2018/01/17	IP	Y	Y	Continuous post	380mg/kg	--	(min 40) stopped breathing, experiment ended	N	--	Y

2018/01/24	IP	Y	Y	Continuous post (15 min)	380mg/kg	--	(min 59) stopped breathing, experiment ended	N	--	Y
2018/02/14	IP	Y	Y	Continuous post (20 min)	380mg/kg	--	(min 3) breathing problems (min 17) breathing stopped (min 18) experiment stopped	N	--	Y
2018/02/21	IP	Y	Y	Continuous post (20 min)	380mg/kg	--	Stable vitals 60 min post-pilo injection	N	--	N
2018/02/28	IP	Y	N **	--	380mg/kg	--	(min 36) stopped breathing, experiment ended	N	--	Y
2018/03/14	IP	Y	Y	Continuous post (0-5 min) (10-20 min)	380mg/kg	--	(min 20) stopped breathing, experiment ended	N	--	Y
2018/03/28	IP	Y	Y	Continuous post (40 min)	380mg/kg	1mg/kg	Stable vitals	Y	257.3	N
2018/04/04	IP	Y	Y	Continuous post (40 min)	380mg/kg	1mg/kg	Stable vitals	N	--	N
2018/04/11	IP	Y	Y	Continuous post (40 min)	380mg/kg	1mg/kg	Stable vitals	Y	117 207	N
2018/04/18	IP	Y	Y	Continuous post (40 min)	380mg/kg	1mg/kg	Stable vitals	N	--	N

* No ECoG was recorded because this experiment was simply to test the transition between drugs to explore if that was a cause of mortality.
** No ECoG was recorded because a glass cover slip was used to visualize changes in angiogram images. Ultimately, the difference in image quality was sacrificed due obtain ECoG analysis.

Appendix B

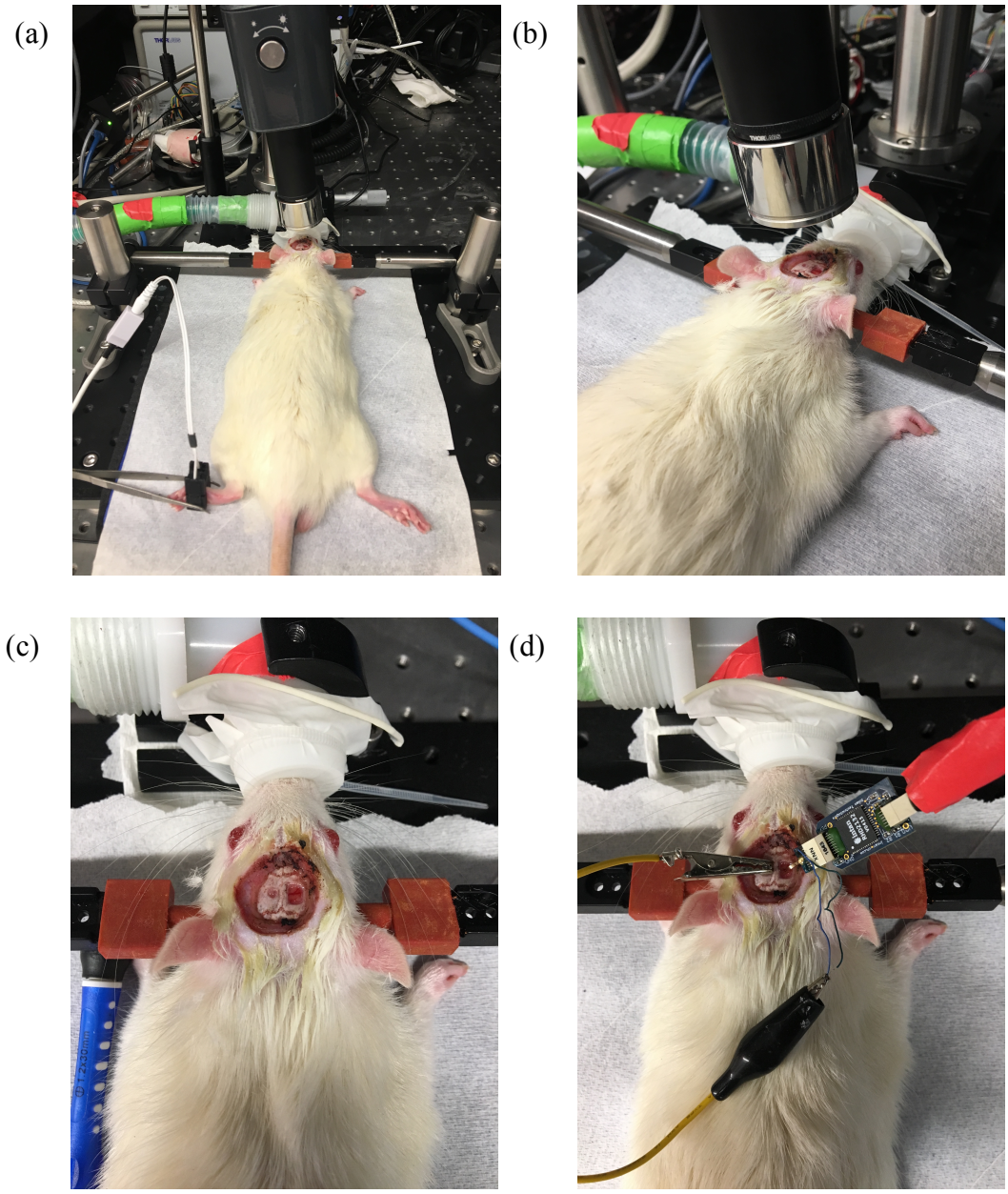

Figure B 1: Images of actual OCT and ECoG setup. (a) OCT setup with probe above cranial imaging window. (b) Side view of OCT setup. (c) Top view of cranial window (right side of skull) and cranial hole for screw (left side of skull). (d) Top view of ECoG setup. ECoG probe shown in contact with the exposed cortex. Screw shown grounded to the ECoG probe by yellow wire and alligator clips.

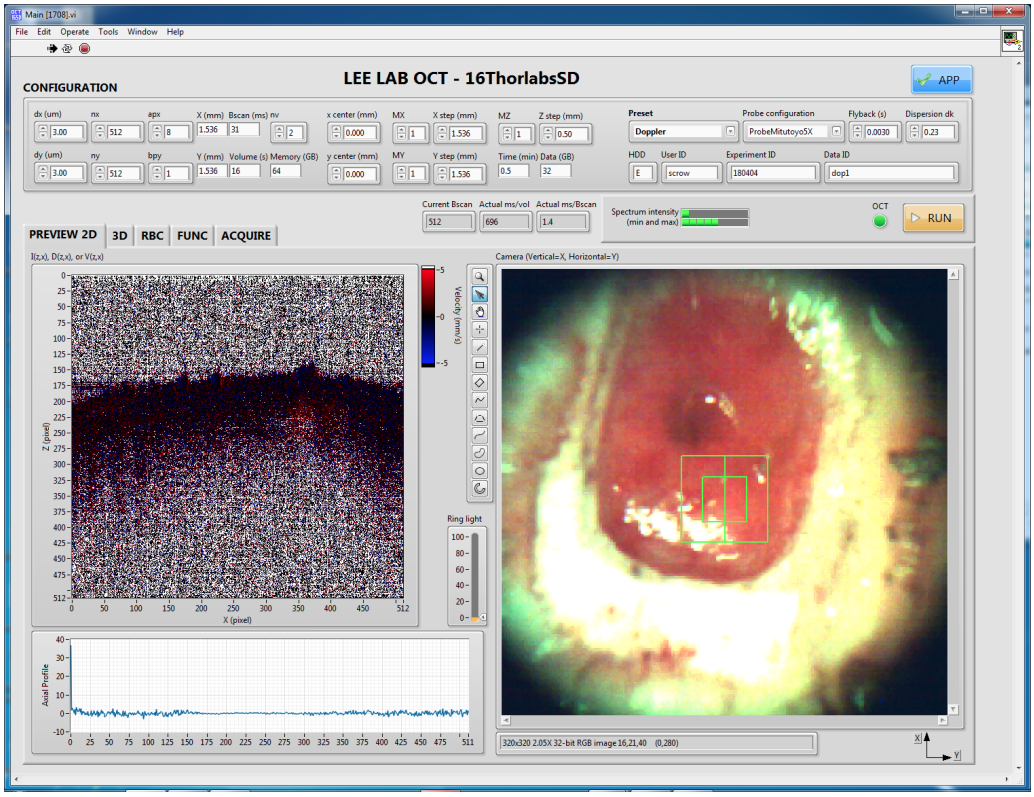

Figure B 2: Screenshot of custom Lee Lab OCT Software. Settings for Doppler OCT.

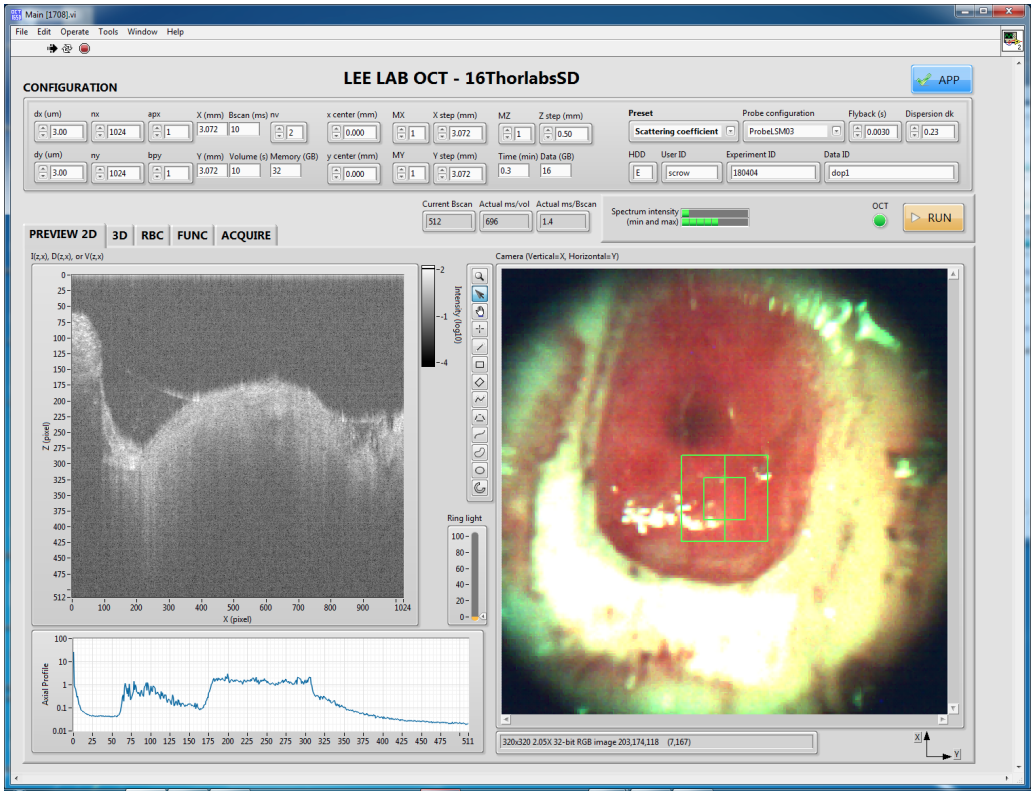

Figure B 3: Screenshot of custom Lee Lab OCT Software. Settings for scattering coefficient OCT.

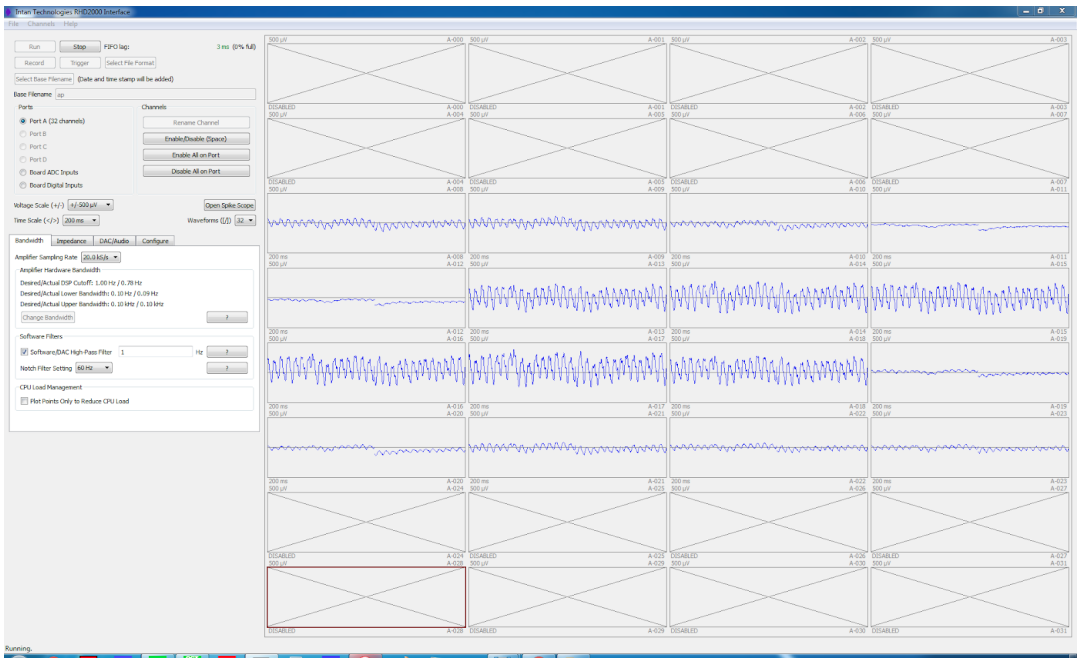

Figure B 4: Screenshot of ECoG data collection software.

```
% load all time points
clear all;
E = cell(2,40);
for i = 1:39
    load (['\\files.brown.edu/Research/ENG_Lee-Lab_Shared/group/data/16ThorlabsSD/scrow/180404_processedECoG/ap_180404_min' num2str(i)])
    E{1,i} = t_amplifier();
    E{2,i} = amplifier_data(1,:);
end
EE = cell2mat(E);

% plot all time points // raw and spectrogram
figure();
plot(EE(1,:),EE(2,:),'k');
ylim([-4000 4000]);
xlim([EE(1,1) EE(1,length(EE))]);
xlabel('Time (sec)');
ylabel('Voltage (uV)');
title('ECoG');

% spectrogram of all time points
figure()
spectrogram(EE(2,:),kaiser(10000,1),500,[],3000,'yaxis')
set(gca,'XTickLabel',[]);
xlabel('Time (min)');
title('Spectrogram');
ylim([0 0.05]);
colormap('jet');
```

Figure B 5: Screenshot of Matlab code to plot ECoG and spectrogram over all time points.

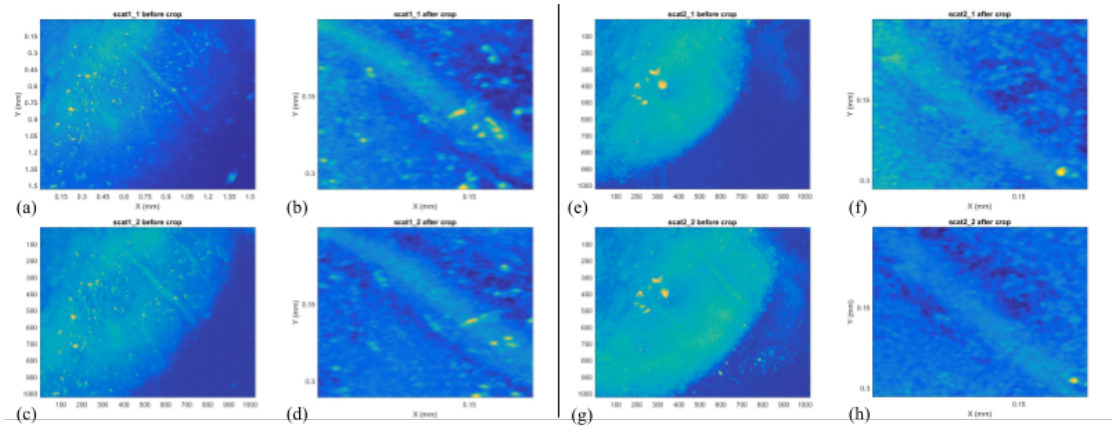

Figure B 6: Selection of scattering coefficient ROI. Experiment date 180328. Scattering coefficient images. scat1 images were taken before pilocarpine injection, while scat2 images were taken after seizure activity. (b,d,f,h) correspond to (a,c,e,g) after selection of ROI.

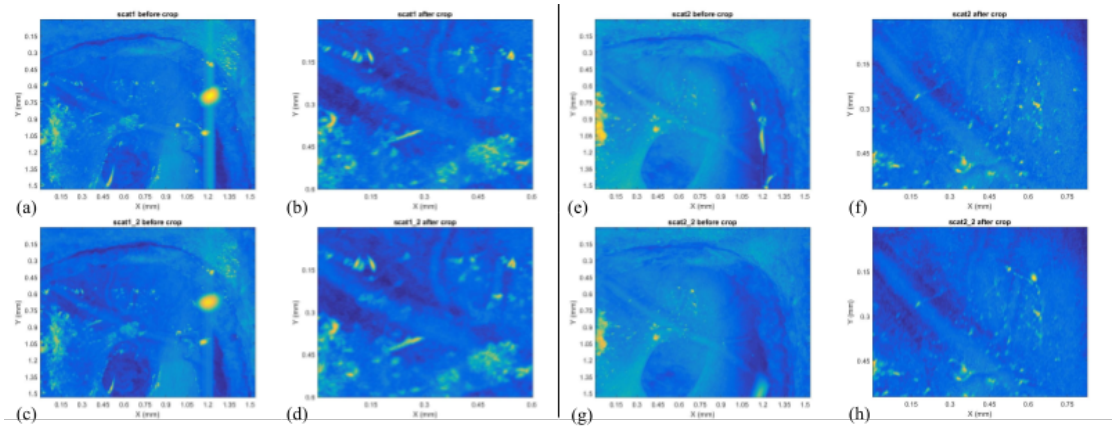

Figure B 7: Selection of scattering coefficient ROI. Experiment date 180404. Scattering coefficient images. scat1 images were taken before pilocarpine injection, while scat2 images were taken after seizure activity. (b,d,f,h) correspond to (a,c,e,g) after selection of ROI.

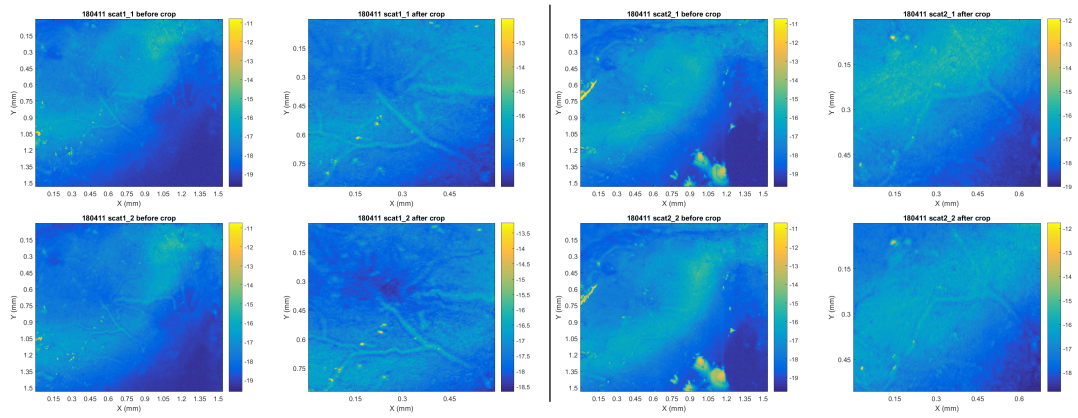

Figure B 8: Selection of scattering coefficient ROI. Experiment date 180411. Scattering coefficient images. scat1 images were taken before pilocarpine injection, while scat2 images were taken after seizure activity. (b,d,f,h) correspond to (a,c,e,g) after selection of ROI.